Summer student project report: Towards measuring the photon polarization in $B^0 \to K_s^0\pi^+\pi^-\gamma$

Murillo Rebuzzi Vellasco
Supervisor: Biplab Dey

September 2018

Abstract

The goal of the project was to study the $B^0 \to K_s^0\pi^+\pi^-\gamma$ decay, which is observed at LHCb, in particular to optimize the background reduction by using PID variables in the training of a BDT on control modes, and also to generate Monte Carlo toy models for the decay. There was a distinct improvement when the PID variables were used in the BDT, and also the amplitude analysis was successful in generating the toys even though we weren't able to perform fits due to time constraints. The results shown are unofficial and have not been formally approved by the LHCb collaboration.

1 Introduction

LHCb is just starting to look at $B^0 \to K_s^0\pi^+\pi^-\gamma$ decays. Underlying this decay is the $b \to s\gamma$ transition, which only occurs via the weak interaction. In the Standard Model (SM), this flavor changing neutral current is forbidden at tree level, thus only occurring through loop level diagrams, such as the one represented by the Feynman diagram in Fig. 1 below.

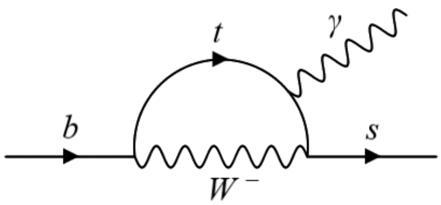

Figure 1: Loop level Feynman diagram for the $b \to s\gamma$ transition.

Also according to the Standard Model, due to the (V-A) structure of the weak interaction (the fact that the W boson is left-handed) and conservation of angular momentum, the photon produced in the $B^0 \to K_s^0\pi^+\pi^-\gamma$ decay is almost fully right-handed, since this will be the case for the transition $\bar{b} \to \bar{s}\gamma$, where γ is almost fully right-handed. In the SM, there is a slight contamination of the opposite helicity, however, since this component is proportional to $(m_s/m_b)^2 \sim \mathcal{O}(10^{-2})$, the square of the ratio of the masses of the corresponding quarks, this effect is very small. Also, we know that the B^0 meson oscillates between itself and its antiparticle (that is, $B^0 \leftrightarrow \overline{B^0}$). The decay considered in this project, $B^0 \to K_s^0\pi^+\pi^-\gamma$, is a decay of the form $B^0 \to f_{CP}\gamma$, where f_{CP} is a CP eigenstate. For decays of this type, it is possible to study time-dependent CP violation (TD-CPV) due to interference of mixing and decay. However, in the decay $B^0 \to K_s^0\pi^+\pi^-\gamma$, the photon has opposite polarization from the one created in the conjugate decay, $\overline{B^0} \to K_s^0\pi^+\pi^-\gamma$, and therefore the two conjugate decays have two different final states, and thus no TD-CPV should be observed (that is, of course, according to the SM). Since many extensions of the standard model account of a higher presence of the opposite helicity of the photon in this decay, a precise measurement of the photon polarization in this decay is very sensitive to new physics.

The project itself was divided into two parts. The first involved developing a procedure to optimize the background reduction in the $B^0 \to K_s^0\pi^+\pi^-\gamma$ decay, by using a BDT including PID variables. This procedure is described in Sec. 2. The second part consisted of using a model for the decay to generate Monte Carlo pseudo-experiments, and is described in Sec. 3.

2 Selection optimization using control modes

2.1 Current state of photon polarization measurements in B factories

LHCb has already probed photon polarization in several modes. The first direct observation of the photon polarization in the $b \to s\gamma$ transition, which had a significance of 5.2σ, was reported by LHCb [1] in a study of the $B^+ \to K^+\pi^-\pi^+\gamma$ decay. This study also analyzed the angular distribution of the emitted photon, that is, the direction that the trajectory of the emitted photon makes in relation to the plane of the four-momenta of the daughter particles, and in particular looked into the *up-down asymmetry* between the number of photons emitted above and bellow this plane. LHCb also made the first experimental observation of the photon polarization in radioactive B_s^0 decays [2], where the $B_s^0 \to \phi\gamma$ decay was studied. Currently, LHCb is performing a time-dependent CP-violation analysis of this decay.

Meanwhile, two other B factories, Belle and BaBar, have also looked into neutral modes. BaBar [3] has studied the $B^0 \to K_s^0\pi^+\pi^-\gamma$ decay with 243 signal events and performed a time-dependent CP-violation analysis of this decay. This is also a very hot topic at Belle II, which is also studying decays such as $B^0 \to K_s^0\pi^0\gamma$.

LHCb is just starting to look at $B^0 \to K_s^0\pi^+\pi^-\gamma$ decays, and considering data collected between 2011-2017 (Run 1 + Run 2 until 2017), a preliminary unoptimized estimate is that 2543 signal events were observed, about ten times more events than BaBar observed in Ref. [3]. However, one major issue is the presence of a large amount of combinatorial background, as can be seen on Fig. 2.

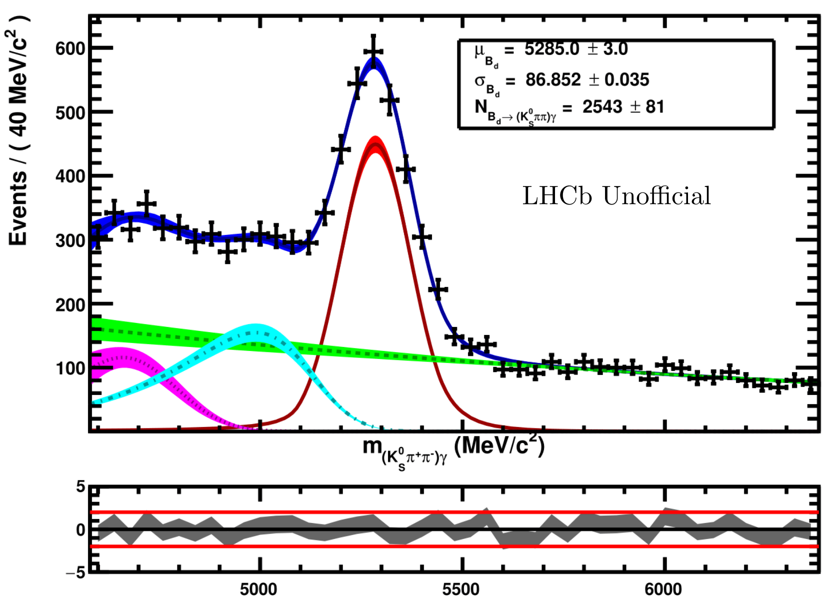

Figure 2: Preliminary study of the data collected by LHCb for the $B^0 \to K_s^0\pi^+\pi^-\gamma$ decay between 2011 and 2017, showing a large amount of combinatorial background, represented by the green strip.

Since there is an ongoing analysis related to this decay, it would be of great interest to develop a procedure to decrease this background yield without affecting the signal yield very much. Preliminary Run 1 studies have shown that for the same signal yield, a BDT (Boosted Decision Tree) based selection, using only kinematic variables, is much cleaner than a cut based one. Using LHCb's powerful PID (Particle Identification) capabilities, we can do better. The goal of this part of the project was to study the effect of the inclusion of PID variables in the training of the BDT, to see if the selection could be improved even further.

2.2 Validation of the use of the BDT using the control modes

PID variables are crucial to identify final states of identical topology. They are used, for example, to separate between kaons (K), pions (π) and protons (p), which can be done using a RICH detector. Our approach to reduce the combinatorial background was therefore to include PID variables in the training of a BDT (along with kinematic variables), and we expected to see an improvement in background reduction over the BDT trained using only kinematic variables. The PID variables we used were of the ProbNN type which, in contrast to pure PID variables (called DLL variables), also include track-wise kinematic variables, χ^2, and ghost probability.

In order to validate the use of the BDTs that would eventually be trained, we considered two high-statistics control modes: $B^0 \to K^*\gamma$ and $B_s^0 \to \phi\gamma$. But before using the PID variables for these decays, it was necessary to correct the PID response for the Monte Carlo (MC) signal samples according to the PID calibration data. This was done using two packages, called PIDGen and PIDCorr. In the former, PID resampling is performed, where the PID response is replaced by one that is generated randomly using specific calibration samples, as a function of track P, PT and how busy the entire event was. In the latter, the MC PID variables are actually transformed in such a way that they will then be distributed according to calibration data, and thereby the signal data. Here, the data used is actually sWeighted data, that is, data on which the sPlot technique [4] was applied in order to subtract the background. Fig. 3 shows the distribution of some ProbNN variables (for the $B^0 \to K^*\gamma$ control mode), and it is clear that the transformed MC PID variables are a better fit to the data than the original variables. Also, it should be noted that the PIDCorr package has the advantage over PIDGen that the correlations between the ProbNN variables are maintained after the transformation. This can be observed on the right plot of Fig. 3, in which the multiplication of the corrected variables is still distributed according to the data.

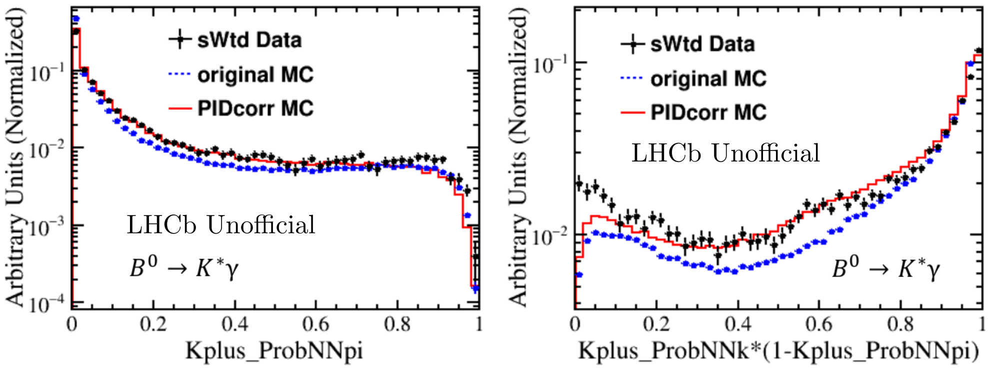

Figure 3: Comparison plots between sWeighted data and corrected MC, for the distribution of the ProbNN variables. Here, the control mode considered is $B^0 \to K^*\gamma$.

The same comparison plots were made for all other PID variables, for both control modes, which also showed that the comparison between sWeighted data and resampled MC is good, as in the plots of Fig. 3.

Two different BDTs were trained: one, which we called the PIDCuts BDT, was trained using only kinematic variables and two cuts on the ProbNN variables (namely, $Kplus\_ProbNNk > Kplus\_ProbNNpi$ and $piminus\_ProbNNpi > piminus\_ProbNNk$). The second one was trained using kinematic variables and ProbNN variables resampled using the PIDGen package, and we therefore called it the PIDGen BDT. It can be seen in Fig. 4 below that the comparison between sWeighted data and resampled MC is good in the BDT directly. We conclude that all correlations among the BDT variables are preserved between data and MC.

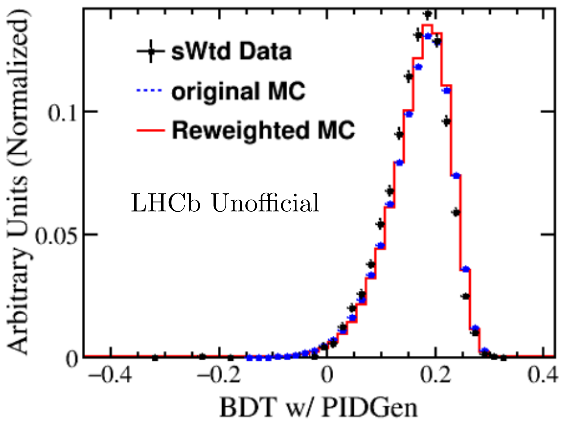

Figure 4: Comparison plot between sWeighted data and reweighted MC on the PIDGen BDT directly (for the $B^0 \to K^*\gamma$ control mode). The correlations between the two ProbNN variables are maintained

2.3 Results for the $B^0 \to K^*\gamma$ control mode

In order to compare the performance of the two BDTs used, we considered two variables, *significance* and *purity*, defined below:

$$Significance = \frac{N_{sig}}{\sqrt{N_{sig} + N_{bkgd}}} \qquad\qquad Purity = \frac{N_{sig}}{N_{sig} + N_{bkgd}} \tag{1}$$

Where N_{sig} is the number of extracted signal events and N_{bkgd} is the number of background events. We considered the optimal BDT to be at the point of maximum significance. For both the PIDGen BDT and the PIDCuts BDT, the BDT cut was varied in steps of 0.035, and the optimal significance was found at $BDT > 0.09$ (for both). A plot for the significance as a function of the BDT cut, for both BDTs, is shown is Fig. 5 below, where it is clear that the significance of the PIDGen BDT is predominantly higher than the one of the PIDCuts BDT.

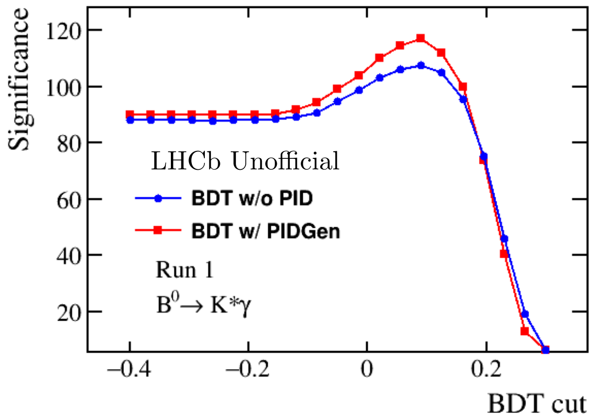

Figure 5: The significance as a function of the BDT cut for both considered BDTs.

Comparing the two performance variables considered at the point of optimal significance ($BDT > 0.09$), shown in Table 1 below, we see that even though the purity was about the same for both BDTs, the significance was, in fact, improved.

	Purity	Significance
BDT w/o PID	0.68604	107.365
BDT w/ PIDGen	0.665492	117.117

Table 1: The value of the performance variables at the point of optimal significance for both BDTs (LHCb Unofficial).

Another way to look for an improvement in the BDT performance was by choosing the cut for each of the two BDTs such that the number of signal events was about the same for both, and checking the corresponding values for N_{bkgd} and the purity. We did this by taking points with $N_{sig} \approx 16820$ for both BDTs. The performance variables at these points are shown in Table 2 below. It is clear that there is a significant improvement in the BDT by using the PID variables: for the same number of signal events, the BDT with PIDGen has about 23.6% less background than the PIDCuts BDT (which is without PID variables). The purity is therefore higher for the PIDGen BDT.

	N_{sig}	N_{sig}	Purity	Significance
BDT w/o PID	16802.4	7689.47	0.68604	107.365
BDT w/ PIDGen	16834.7	5867.56	0.741543	111.730

Table 2: A comparison between the performance variables for the two BDTs at point with about the same N_{sig} (LHCb Unofficial).

Fig. 6 below shows the distribution of the $m_{K\pi\gamma}$ variable of the data set with a cut on the PIDCuts BDT (on the left) and PIDGen (on the right), such that for both $N_{sig} \approx 16820$. It should be noted how the background is reduced when we switch from the PIDCuts BDT to the PIDGen one.

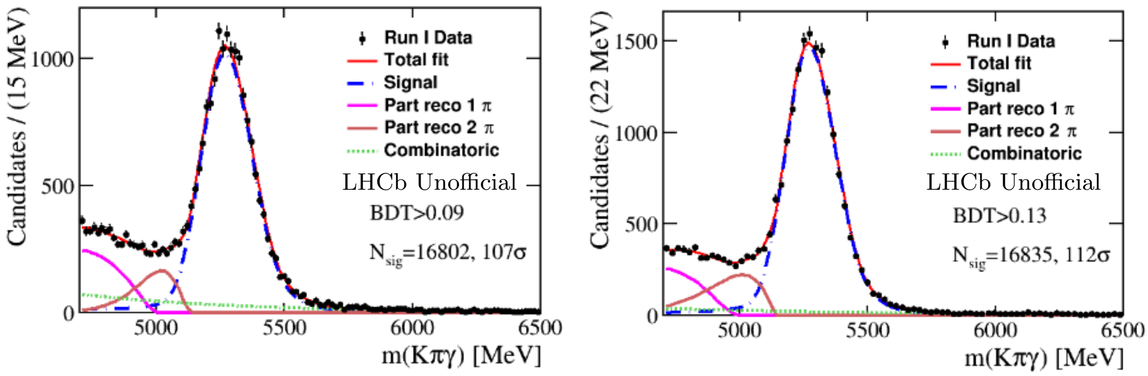

Figure 6: Comparison of the BDT performance with and without PID. On the left, the BDT used was the PIDCuts BDT (where the purity is 68.6% and the significance is 107σ), while on the right the PIDGen BDT was used (where the purity is 74.2% and the significance is 112σ).

The same procedure was taken for the second control mode, $B_s^0 \to \phi\gamma$, and the results obtained also indicated an improvement in performance when the PID variables were used in the BDT.

3 Amplitude analysis

One of the main goals of the project was to develop the code to generate Monte Carlo toy models for the $B^0 \to K_s^0\pi^+\pi^-\gamma$ decay. In order to do this, it was necessary to have an expression for the decay rate of this process, which is a product of the modulus of the amplitude for the decay squared and the phase space element. In order to obtain the amplitude, we followed the steps of a paper [3] by the BaBar collaboration, and for the phase space element, which Ref [3] didn't take into consideration, we developed a parametrization in terms of Legendre polynomials.

3.1 Decay resonances

Following Ref. [3], even though our goal was to study the neutral mode $B^0 \to K_s^0\pi^+\pi^-\gamma$, this decay has too many resonances in the $(K_s^0\pi^+\pi^-)$ system and the construction of the amplitude is much too complicated. Instead, we constructed the amplitude corresponding to the charged mode $B^+ \to K^+\pi^+\pi^-\gamma$ which, due to isospin symmetry, is proportional to the neutral mode amplitude. This choice is further justified by the fact that the charged mode has higher statistics in B factories such as LHCb, BaBar and Belle, than the neutral mode.

The amplitude for the charged mode is modeled by intermediate decay resonances in the $(K\pi\pi)$, $(K\pi)$ and $(\pi\pi)$ systems. On the $m_{K\pi\pi}$ spectrum, five resonances were considered, listed in Table 3 below.

J^P	K_{res}	Mass m^0 (MeV/c^2)	Width Γ^0 (MeV/c^2)
1^+	$K_1(1270)$	1272 ± 7	90 ± 20
	$K_1(1400)$	1403 ± 7	174 ± 13
1^-	$K^*(1410)$	1414 ± 15	232 ± 21
	$K^*(1680)$	1717 ± 27	322 ± 110
2^+	$K_2^*(1430)$	1425.6 ± 1.5	98.5 ± 2.7

Table 3: The resonances considered on the $m_{K\pi\pi}$ spectrum

Each of the resonances was parametrized by a relativistic Breit-Wigner function R_k with constant width Γ^0, whose expression is the following:

$$R_k^J(m) = \frac{1}{(m_k^0)^2 - m^2 - im_k^0\Gamma_k^0} \tag{2}$$

The amplitude squared of the $m_{K\pi\pi}$ spectrum is then given by the following expression:

$$|A(m; c_k)|^2 = \sum_{J^P} \left| \sum_k c_k R_k^J(m) \right|^2, \tag{3}$$

where contributions from different spin-parity resonances do not interfere, since the analyzing direction of the photon is summed over. For the $m_{K\pi}/m_{\pi\pi}$ spectra, three resonances were used. Their parameters and respective parametrizations are given on Table 4 below:

J^P	Resonance	Parameters	Analytical Expression
1^-	$K^*(892)$	$m_0 = 895.94 \pm 0.22$ $\Gamma_0 = 50.8 \pm 0.9$ $r = 3.6 \pm 0.6$	RBW
1^-	$\rho(770)$	$m_0 = 775.49 \pm 0.34$ $\Gamma_0 = 149.1 \pm 0.8$ $r = 5.3^{+0.9}_{-0.7}$	GS
0^+	$K_0^*(1430)$	$m_0 = 1425 \pm 50$ $\Gamma_0 = 270 \pm 80$	RBW

Table 4: The resonances considered on the $m_{K\pi}/m_{\pi\pi}$ spectrum

In Table 4, RBW stands for relativistic Breit-Wigner, and GS stands for the Goursaris-Sakurai parametrization. For the $K^*(892)$ resonance, a relativistic Breit-Wigner with a mass-dependent width $\Gamma(m)$ was used, according to Ref. [3]. However, for the $K_0^*(1430)$ resonance, a simple relativistic Breit-Wigner with constant width was used, for simplicity, due to time constraints on the project, even though Ref. [3] uses the LASS parametrization. Both the GS and RBW with mass-dependent width $\Gamma(m)$ parametrizations are given in App. A.

Given the amplitudes for the $m_{K\pi\pi}$ and $m_{K\pi}/m_{\pi\pi}$ spectra, the total amplitude used for the charged mode decay was the product of these separate amplitudes.

3.2 Phase space parametrization

The other crucial step to generating toy models was obtaining an expression for the phase space. Our first option was to use the ROOT library `TGenPhaseSpace`, which generates events and calculates the phase space element using the four-momenta of daughter particles. Given this element and the modulus squared of the amplitude, we could weigh each event by the total decay rate, and therefore we were able to generate Monte Carlo events that simulate the actual decay. However, there was one major drawback; in order to construct a probability density function for the decay, an analytical expression for the phase space element was needed (which we had for the total amplitude), and it is not possible to obtain this expression from `TGenPhaseSpace`.

We then tried searching for an analytical expression for the phase space, however, we weren't successful. The decay we were studying is a 4-body decay, which is 7-dimensional: $m_{K\pi\pi}$, $m_{K\pi}$, $m_{\pi\pi}$, $m_{\gamma\pi\pi}$, $m_{\gamma\pi}$ and two other angular variables; it is unfortunately too complicated. Since an analytical expression was not available, we decided to parametrize the phase space as a linear combination of Legendre polynomials. The choice of these polynomials was made because they are complete (so that any sufficiently smooth function can be written as a linear combination of them) and orthogonal, which allows us to calculate the linear combination coefficients by performing a simple integration. For simplicity, we chose to use a 3-dimensional phase space, using the variables $m_{K\pi\pi}$, $m_{K\pi}$, and $m_{\pi\pi}$.

The procedure worked as follows: we parametrized the phase space element as a linear combination of the Legendre polynomials until a certain maximum order. Then, we generated events according to the actual phase space using `TGenPhaseSpace`. Finally, we were able to extract the coefficients of the linear combination by calculating the integrals numerically using the generated data. The phase space element was then given by:

$$\begin{aligned} d\Omega_{4-body}(m^*_{K\pi\pi}, m^*_{K\pi}, m^*_{\pi\pi}) &= f(m^*_{K\pi\pi}, m^*_{K\pi}, m^*_{\pi\pi}) dm^*_{K\pi\pi} dm^*_{K\pi} dm^*_{\pi\pi} \\ f(m^*_{K\pi\pi}, m^*_{K\pi}, m^*_{\pi\pi}) &= \sum_{i=1}^{n_{K\pi\pi}} \sum_{j=1}^{n_{K\pi}} \sum_{k=1}^{n_{\pi\pi}} c_{ijk} P_i(m^*_{K\pi\pi}) P_j(m^*_{K\pi}) P_k(m^*_{\pi\pi}) \end{aligned} \tag{4}$$

In the equation above, c_{ijk} is a constant coefficient and P_i is the Legendre polynomial of order i. The integer $n_{K\pi\pi}$ is the maximum order of polynomials in the $m_{K\pi\pi}$ variable (and analogously for the other variables). Finally, the reason why all the variables are primed is that the domain of the Legendre polynomials is the interval $[-1, 1]$, so that all three variables had to be rescaled to that interval, that is, $-1 \leq m_{K\pi\pi} \leq 1$ and so on. From the orthogonality of the Legendre polynomials, we know that:

$$c_{ijk} = \left(\tfrac{2i+1}{2}\right)\left(\tfrac{2j+1}{2}\right)\left(\tfrac{2k+1}{2}\right)\int_{-1}^{1}\int_{-1}^{1}\int_{-1}^{1} f(m^*_{K\pi\pi}, m^*_{K\pi}, m^*_{\pi\pi})P_i(m^*_{K\pi\pi})P_j(m^*_{K\pi})P_k(m^*_{\pi\pi})dm^*_{K\pi\pi}dm^*_{K\pi}dm^*_{\pi\pi} \quad (5)$$

This integration, however, can be performed numerically using the data generated with *TGenPhaseSpace*, without the knowledge of the function f (which, in fact, is what we are trying to find out). Therefore, all the coefficients c_{ijk} can be extracted from the Monte Carlo data.

Finally, after we obtained this parametrization, we performed some cuts in order to exclude the unphysical regions of the phase space. That is, if a point in the phase space is unphysical (in other words, not kinetically allowed), we set the phase space element to zero. The cuts we performed, based on Ref. [5], are:

$$m_{K\pi} \geq m_k + m_\pi \quad (6)$$
$$m_{\pi\pi} \geq m_\pi + m_\pi \quad (7)$$
$$m_{K\pi\pi} \geq m_{K\pi} + m_\pi \quad (8)$$
$$m_{K\pi\pi} \geq m_K + m_{\pi\pi} \quad (9)$$
$$G(m^2_{K\pi}, m^2_{\pi\pi}, m^2_{K\pi\pi}, m^2_\pi, m^2_K, m^2_\pi) \leq 0 \quad (10)$$

Where $m_K = 493.677\ MeV/c^2$ is the mass of K^+, $m_\pi = 139.570\ MeV/c^2$ is the mass of π^+ and the function G is defined as follows:

$$\begin{aligned} G(x, y, z, u, v, w) = \quad & x^2y + xy^2 + z^2u + zu^2 + v^2w + vw^2 + xzw + xuv \\ & + yzw + yuw - xy(z + u + v + w) \\ & - zu(x + y + v + w) - vw(x + y + z + u) \end{aligned} \quad (11)$$

If any of these inequalities wasn't satisfied, the phase space element was set to zero.

3.3 Results

Firstly, in order to validate our phase space parametrization, we performed the method described in Sec. 3.2, using Legendre polynomial up to order 15, to obtain the analytical expression for the 4-body phase space. In Fig. 7 we show the comparison between Monte Carlo data distributed according to the phase space element calculated using `TGenPhaseSpace`, on the left, and using our phase space parametrization, on the right, and it is clear that this method for obtaining an analytical expression for the phase space element was successful, as the two distributions are very similar. The $m_{K\pi\pi}$ distribution was also validated accordingly. Moreover, it would be possible to increase the accuracy of the parametrization by increasing the maximum order of the polynomials used, if necessary.

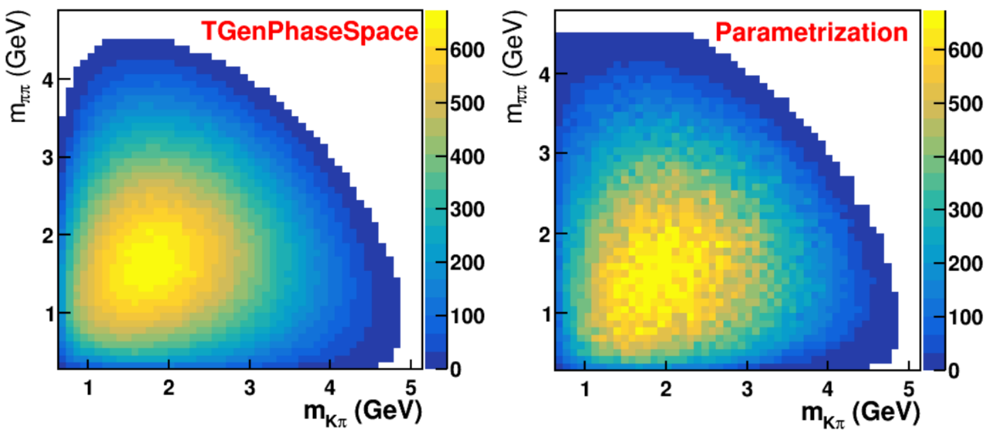

Figure 7: A comparison between the actual 4-body phase space (generated using `TGenPhaseSpace`) and the parametrized phase space, where we chose $n_{K\pi\pi} = n_{K\pi} = n_{\pi\pi} = 15$.

Given the total amplitude (described in Sec. 3.1) and the phase space element (described in Sec. 3.2), we were able to generate Monte Carlo events to simulate the decay. In Fig. 8, we show the results for a single simulated toy model for the decay, where each resonance is pointed out individually. The plot obtained for the $m_{K\pi\pi}$ distribution does match the one present in Ref. [3], so we consider our model to be successful in reproducing the model in that paper.

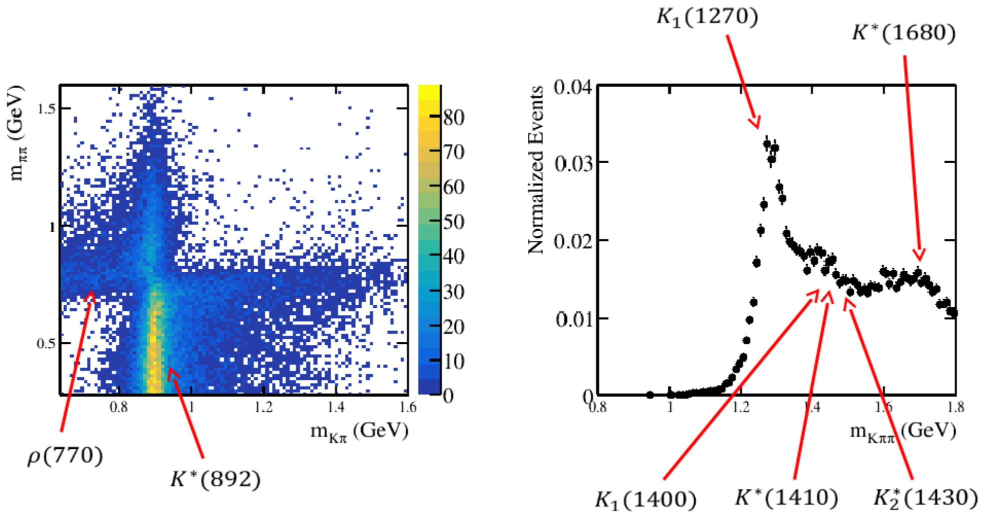

Figure 8: Invariant mass plots for a single toy model generated for $B \to K_J^*(\to K\pi\pi)\gamma$, with the resonances pointed out.

Due to time constraints, we weren't able to successfully converge fits using this amplitude analysis model. We had some issues with the code and weren't able to debug it in time before the end of the summer studentship. However, we believe that this is a minor issue that can be fixed through a careful review of the code.

4 Conclusion

The work done on the selection optimization validated the use of the BDT including ProbNN PID variables on the control modes. A distinct improvement was observed over cut-based analysis, by inclusion of the PID variables. The same procedure for the $B^0 \to K_s^0\pi^+\pi^-\gamma$ signal mode is expected to give optimal background reduction since the topology other than the K_s^0 is the same. The results shown are unofficial and have not been formally approved by the LHCb collaboration.

Regarding the amplitude analysis, the BaBar [3] model was coded up, including the phase space parametrization by Legendre polynomials, which compares fairly well with the actual phase space. However, there is still work to be done in order to be able to perform fits and check the pull distributions.

5 Acknowledgements

Firstly I would like to express my gratitude to my supervisor Biplab Dey, who guided me through the project with tremendous patience and devoted a great amount of time to answering any questions I would have. I would also like to thank the Summer Student Team, who would promptly answer any questions and solve any issues I would have during the summer. Finally, I would like to thank the LHCb collaboration and CERN for giving me such an extraordinary opportunity which was greatly appreciated.

A Appendix: the RBW and GS parametrizations

The *relativistic Breit-Wigner* (RBW) function with a mass-dependent width is given by:

$$R_J(m) = \frac{1}{(m_0^2 - m^2) - im_0\Gamma(m)} \tag{12}$$

For a general spin-J resonance, the width is given by:

$$\Gamma(m) = \Gamma_0 \left(\frac{|\mathbf{q}|}{|\mathbf{q}|_0}\right)^{2J+1} \left(\frac{m_0}{m}\right) \frac{X_J^2(|\mathbf{q}|r)}{X_J^2(|\mathbf{q}|_0)r)} \tag{13}$$

In Eq. 13, r is the Blatt-Weisskopf barrier radius (a given parameter for each resonance), $\mathbf{q}$ is the momentum of one of the daughter particles, in the resonance rest frame. It is a function of the mass m and the masses of the two daughters, m_a and m_b, and is given by:

$$|\mathbf{q}| = \frac{m}{2}\left(1 - \frac{(m_a+m_b)^2}{m^2}\right)^{1/2}\left(1 - \frac{(m_a-m_b)^2}{m^2}\right)^{1/2} \tag{14}$$

Then, $|\mathbf{q}|_0$ is a symbol for this function evaluated at $m = m_0$: $|\mathbf{q}|_0 = |\mathbf{q}|(m_0)$
Finally, the function $X_J^2(|\mathbf{q}|r)$ is the Blatt-Weisskopf barrier factor. For $J = 1$, it is given by (defining $z = |\mathbf{q}|r$ and $z_0 = |\mathbf{q}|_0 r$):

$$X_{J=1}(z) = \sqrt{\frac{1+z_0^2}{1+z^2}} \tag{15}$$

On the other hand, the Goursaris-Sakurai (GS) parametrization for the ρ^0 resonance is given by:

$$R_J(m) = \frac{1 + C \cdot \Gamma_0/m_0}{(m_0^2 - m^2) + f(m) - im_0\Gamma(m)} \tag{16}$$

In Eq. 16 above, $\Gamma(m)$, the mass-dependent width, has the same expression as the one for the RBW parametrization (Eq. 13). Also, we have:

$$f(m) = \Gamma_0 \frac{m_0^2}{q_0^3}\left[q^2(h(m) - h(m_0)) + (m_0^2 - m^2)q_0^2 \left.\frac{dh}{dm^2}\right|_{m=m_0}\right] \tag{17}$$

$$C = \frac{3}{\pi}\frac{m_\pi^2}{q_0^2}\ln\left(\frac{m_0 + 2q_0}{2m_\pi}\right) + \frac{m_0}{2\pi q_0} - \frac{m_\pi^2 m_0}{\pi q_0^3} \tag{18}$$

In the expressions above, we simplified our notation by using $q = |\mathbf{q}|$ and $q_0 = |\mathbf{q}|_0$. Finally, the function $h(m)$ is given by (for $m > 2m_\pi$):

$$h(m) = \frac{2}{\pi}\frac{q}{m}\ln\left(\frac{m+2q}{2m_\pi}\right), \tag{19}$$

where:

$$\left.\frac{dh}{dm^2}\right|_{m=m_0} = h(m_0)\left(\frac{1}{8q_0^2} - \frac{1}{2m_0^2}\right) + \frac{1}{2\pi m_0}. \tag{20}$$

References

[1] The LHCb collaboration. "Observation of photon polarization in the $b \to s\gamma$ transition". In: *Phys. Rev. Lett.* 112, 161801 (2014). DOI: 10.1103/PhysRevLett.112.161801.

[2] The LHCb collaboration. "First experimental study of photon polarization in radiative B_s^0 decays". In: *Phys. Rev. Lett.* 118, 021801 (2017). DOI: 10.1103/PhysRevLett.118.021801.

[3] The BABAR collaboration. "Time-dependent analysis of $B^0 \to K_s^0\pi^-\pi^+\gamma$ decays and studies of the $K^+\pi^-\pi^+$ system in $B^+ \to K^+\pi^-\pi^+\gamma$ decay". In: *Phys. Rev. D* 93, 052013 (2016). DOI: 10.1103/PhysRevD.93.052013.

[4] M. Pivk and F.R. Le Diberder. "sPlot: a statistical tool to unfold data distributions". In: *Nucl. Instrum. Meth.* A555:356-369 (2005). DOI: 10.1016/j.nima.2005.08.106.

[5] Byckling, E. and Kajantie, K. *Particle kinematics.* New York: John Wiley and Sons, 1973, pp. 105-107